Neurobiology of Aging, Vol. 12, pp. 543–556. © Pergamon Press plc, 1991. Printed in the U.S.A. 0197-4580/91 $3.00 + .00

Different Rates of Age-Related Loss For Four Murine Monoaminergic Neuronal Populations

WILLIAM G. TATTON,*[1] CAROL E. GREENWOOD,† MARY C. VERRIER,‡
DIANNE P. HOLLAND,* MAE M. KWAN* AND FRED E. BIDDLE§

*Departments of *Physiology, †Nutritional Sciences and ‡Rehabilitation Medicine*
University of Toronto, Toronto, Ontario
and §Department of Medical Biochemistry University of Calgary, Calgary, Alberta

Received 29 June 1990; Accepted 13 May 1991

TATTON, W. G., C. E. GREENWOOD, M. C. VERRIER, D. P. HOLLAND, M. M. KWAN AND F. E. BIDDLE. *Different rates of age-related loss for four murine monoaminergic neuronal populations.* NEUROBIOL AGING **12**(5) 543–556, 1991.— The age-related loss of locus coeruleus (LC) noradrenergic neurons, substantia nigra compacta (SNc) dopaminergic neurons, dopaminergic retinal amacrine (rAm) neurons and raphe serotonergic neurons, identified using antibodies against tyrosine hydroxylase (TH) and serotonin (5HT) was investigated in C57Bl mice aged 8 to 104 weeks. The neuronal somata were counted and their locations three-dimensionally reconstructed from serial sections alternately immunoreacted or Nissl stained. Nonlinear estimation analysis showed that decaying exponential equations best fitted the plots of neuronal numbers versus age and each subtype was lost according to different exponential constants of −0.015, −0.013, −0.004 and −0.001 for LC TH+, SNc TH+, rAm TH+ and raphe 5HT+ neurons, respectively. Neurons were lost from all different subregions within the nuclei or the retinae. Counts of immediately adjacent TH-immunoreacted and Nissl-stained sections through the LC at different ages indicate that the neuronal loss was due to neuronal death rather than loss of TH immunoreactivity. The markedly different rates of age-related neuronal loss for the four monoaminergic subtypes offer a model to study the underlying molecular and cellular mechanisms.

Aging Neuronal death Substantia nigra Locus coeruleus Raphe nucleus Retinal amacrines

DECREASES in neuronal numbers have been proposed as the major cause of diminished brain function in old age for a century. Yet the extent and time course of age-related neuronal loss (ARNL) remain uncertain (4). Similarly, decreases in a variety of subcellular or chemical indices in the aging brain such as regional transmitter concentrations, decreases in synaptic densities or altered receptor binding have been correlated to diminished behavioral capacities (37). Yet it is not known whether those changes primarily reflect neuronal death or whether they are the result of age-related dysfunction in surviving neurons. Quantitative measures of the extent and time course of the age-related of identified neuronal population are an essential prerequisite to differentiating the roles of neuronal loss and neuronal dysfunction in the causation of subcellular and chemical changes in the aging brain.

Reports of the extent of neuronal loss for specific brain structures in the same species have varied markedly (6). Findings ranging from no neuronal loss to 60% loss or more with aging can be found for most cortical and subcortical structures (4). Determination of the extent of ARNL has been complicated by the indistinct boundaries of some structures which have required that neuronal densities be measured rather than absolute cell counts. Density measures can underestimate neuronal loss if there is tissue shrinkage (13) and some recent studies, attempting to correct neuronal density measures for tissue shrinkage, have calculated little or no neuronal loss with aging in structures previously considered to undergo significant loss (34).

It is believed that different neuronal populations are lost to different extents with aging (4) which may underlie the nonuniform reductions seen in different behavioral capacities with aging. Full evaluation of differential neuronal loss with aging would require the identification of what might be termed behaviorally specific or functionally related neuronal subtypes. This could require the concurrent examination of numerous neuronal identification criteria like brain region, origins and destinations of input and output connections, somal size, dendritic tree shape and extent, types of membrane receptors, transmitter content and the timing of action potential or synaptic activity with respect to defined behavioral parameters. Although extensive identification is impractical for multiple time point studies of brain aging, functionally similar neurons within a given brain structure often utilize the same transmitter(s) (26). Hence identification based on the immunocytochemical identification of transmitter subtypes in a specific region or structure can offer a practical alternative (4,23).

Finally, the time course of ARNL across mammalian life spans remains uncertain (19). Some studies indicate that ARNL is largely restricted to old age and is best represented by two relationships with the second relationship having a considerably steeper slope for the later portions of life [see (35) for an example]. Other investigations of the same neuronal populations (16) appear to show a continuous, almost linear loss throughout life.

[1]Requests for reprints should be addressed to William G. Tatton, Center for Research in Neurodegenerative Diseases, University of Toronto, Tanz Neuroscience Building, 6 Queen's Park Crescent West, Toronto, Ontario, M5S 1A8.

In order to provide a base to interpret subcellular or chemical changes in an aging brain [see (10)], we have determined the extent and time course of ARNL for four different monoaminergic neuronal subtypes in isogenic C57 black mice at multiple time points from 8 weeks of age to 104 weeks of age. Counts from alternate serial sections or retinal whole mounts revealed different time courses of ARNL for each subtype and showed that the neuronal loss involved all parts of each nucleus or retina. The ARNL could be best characterized by a simple decaying exponential equation for each of the four subtypes.

METHOD

C57BL/6 mice were obtained from an isogenic colony at the University of Calgary (n = 46) or from the National Institutes of Aging colony at the Jackson laboratories (n = 20). The mice from the two sources were originally from the same stock approximately 40–60 generations previously. The University of Calgary mice were maintained in boxes protected from airborne pathogens with filter hoods and semisterile procedures were followed so as not to transmit any pathogens from other mouse stocks held in the same facilities. The age of the Calgary mice was taken from the day of birth and animals sacrificed at a variety of ages from 8 weeks to 104 weeks depending on space needs in the colony. Mice from the Calgary colony were observed daily and were not included in the study if they were ill or showed behavioral abnormalities at any time during their lives. The NIA mice were sacrificed within one week of receipt from the Jackson laboratories and were only specified as to months of age (2, 5, 11, 20 or 24 months of age).

The mice were anaesthetized with pentobarbital and then were perfused through the ascending aorta with 4% paraformaldehyde in 0.1 M phosphate buffer. Following perfusion the thoracic and abdominal cavities were examined for any gross pathology. Brain tissue from animals with any gross pathology was not included in the study.

The intact retinae were dissected from the eyes leaving the pigment epithelium behind and were treated with 1% Triton X-100 and 1% DMSO to facilitate penetration of the antiserum into the uncut cells in the whole mounts. Whole mounts were incubated for up to 5 days at 4°C with primary antisera [1:500 tyrosine hydroxylase (TH) polyclonal antisera from Eugene Tech] which was replaced after 2–3 days [see (33) for more details].

The perfused brains were immersed in 4% paraformaldehyde in 0.1 M phosphate buffer overnight and then were placed in 20% sucrose. Serial frozen sections, 20 microns in thickness, were cut in the frontal plane through the brainstem and diencephalon so as to include all of the SNc, the LC and the raphe nucleus. In some animals, sections were only taken through the mescencephalon and the pons for the SNc and LC nuclei or alternately through the lower pons and the medulla for the raphe neurons.

Alternate sections were Nissl stained or reacted immunocytochemically for TH or serotonin (5HT, Incstar) antibodies and then visualized with the avidin-biotin method (ABC Kit, Vector Labs) using diaminobenzidine (DAB) as the chromogen [see (31) for further details]. Slide-mounted or floated sections were incubated with primary antisera overnight. Tissues were washed with phosphate buffer then incubated in biotinylated goat anti-rabbit IgG secondary antibody followed by avidin-HRP incubation. A 0.05% solution of DAB in 0.01% hydrogen peroxide was used to visualize the immunoreactive cells and processes. Controls incubated with nonimmune serum in place of primary antiserum were treated similarly and were found to be nonreactive.

The total number of TH+ retinal amacrines were counted for each retina and divided by the area of the retina to obtain somata/mm^2. The counts of TH+ retinal amacrines were unambiguous since each soma and its processes could be viewed in the whole mounts. Counts of TH+ or 5HT+ somata on number-coded alternate serial sections through the complete nucleus were made for each of the monoaminergic populations. Counts were only made of TH+ profiles which contained a immunolucent region compatible with a nucleus that contained a nucleolus when examined with our interference contrast optics. This procedure avoided the possibility of mistaking neuronal somata for somal or process fragments. Sections were recounted by two different observers who were blind to the animals' ages to check for any observer bias. The values were corrected for section thickness and the fact that alternate sections were counted (17) and were expressed as a percentage of the mean number determined for the 8-week-old animals.

The somal locations for the immunochemically identified neurons were three-dimensionally reconstructed on a PDP 11/30 computer from the serial alternate sections for representative nuclei [see (29,31) for details]. Somal distribution plots were constructed for cell numbers versus section number longitudinally along the brainstem relative to specific landmarks taken from the alternate Nissl sections. The two procedures were used to determine if any loss of immunopositive somata was accentuated in any subregion of the nuclei.

The alternate Nissl sections were also used to compare the numbers of TH+ neuronal somata and the numbers of Nissl-stained neuronal somata for immediately adjacent alternate sections in the LC. The numbers of TH+ and Nissl neuronal somata on the adjacent sections within the outer nuclear borders determined for the TH+ reacted section were plotted against each other and the relationship of the distribution of the points to the equal number diagonal was examined. The technique provides a means of differentiating reductions of numbers of TH+ neurons caused by a failure of neurons to express immunoreactive TH from that caused by the destruction of neurons that accompanies cell death [see (31) for details of the technique]. Neuronal somata and glial cells were differentiated on the Nissl sections using cross-sectional area criteria for somata which included a nucleolus. A major mode at 50 μm^2 (extending from 30 μm^2 to 90 μm^2) was identical in the young and old animals. These smaller profiles were similar to those described for the rat SNc (27) and were taken to represent glia. Larger profiles ranging in size from 120 μm^2 to 410 μm^2 on both the TH-immunoreacted sections and the Nissl sections were taken to represent neuronal somata.

The values for the somal counts at different ages were anal-

FACING PAGE

FIG. 1. Photomicrographs of representative sections showing TH-immunoreacted SNc neurons at 8 weeks (A1 and A2) and 81 weeks of age (B1 and B2). A1 and B1 were photographed with bright-field optics (scale bar = 200 μm) and A2 and B2 with interference contrast optics (scale = 20 μm). In this figure and Figs. 2, 3 and 4, the low power views were photographed with bright-field illumination to optimally reveal the relative immunodensities in the neuronal somata and appendages while the high power views were taken using interference contrast optics in order to discern cellular borders for both immunoreactive and unreacted somata and processes. Note the relative decrease in the numbers of TH+ neurons in the 81-week SNc compared to the 8-week SNc and the apparent preservation of TH immunodensity in the aged neurons somata and processes.

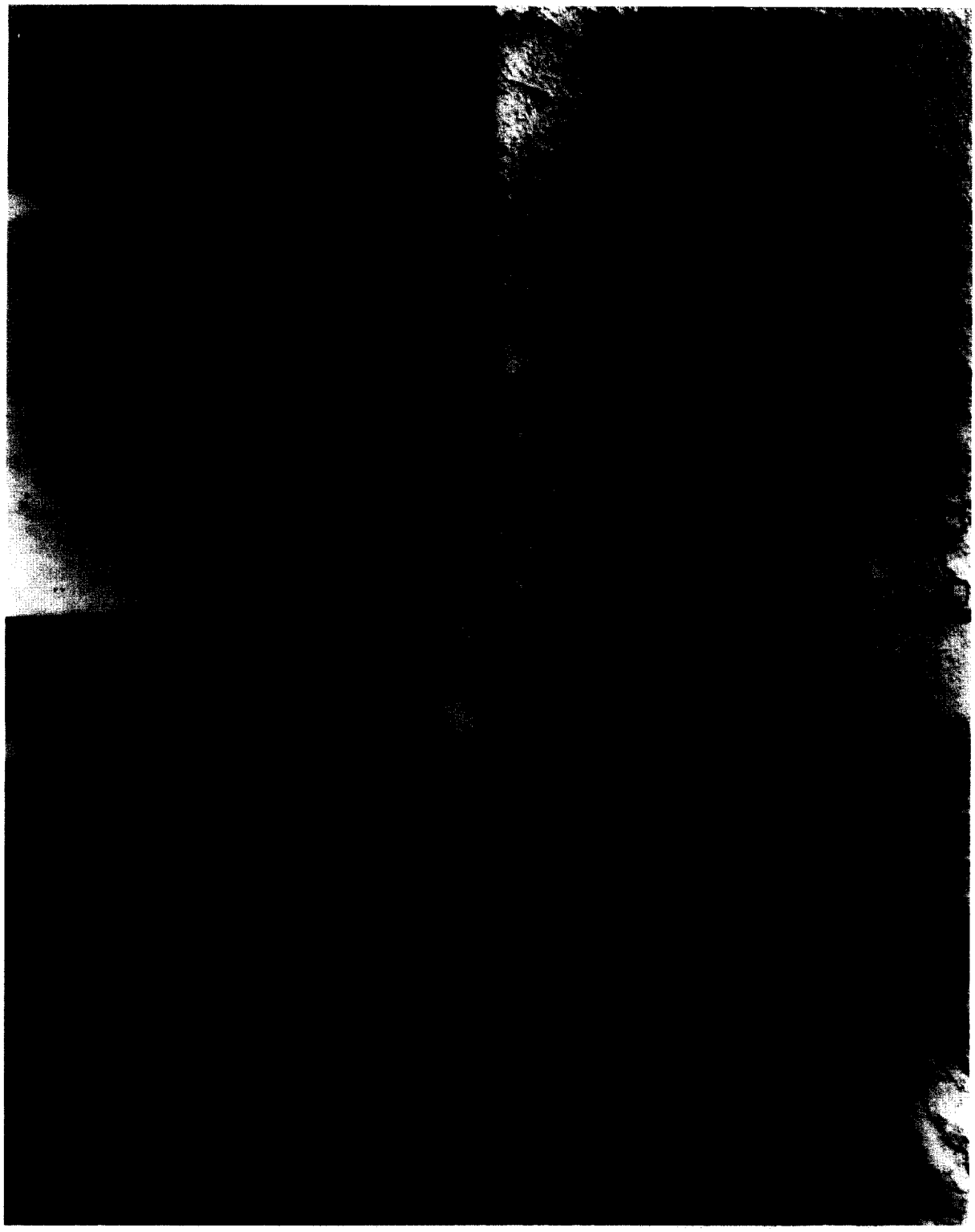

FIG. 2. Photomicrographs of representative sections showing TH-immunoreacted LC neurons at 8 weeks (A1 and A2) and 81 weeks of age (B1 and B2). A1 and B1 used bright-field optics (scale = 200 μm) and A2 and B2 used interference contrast optics (scale = 20 μm). Note the decrease in the numbers of TH+ neurons in the 81-week LC compared to the 8-week LC.

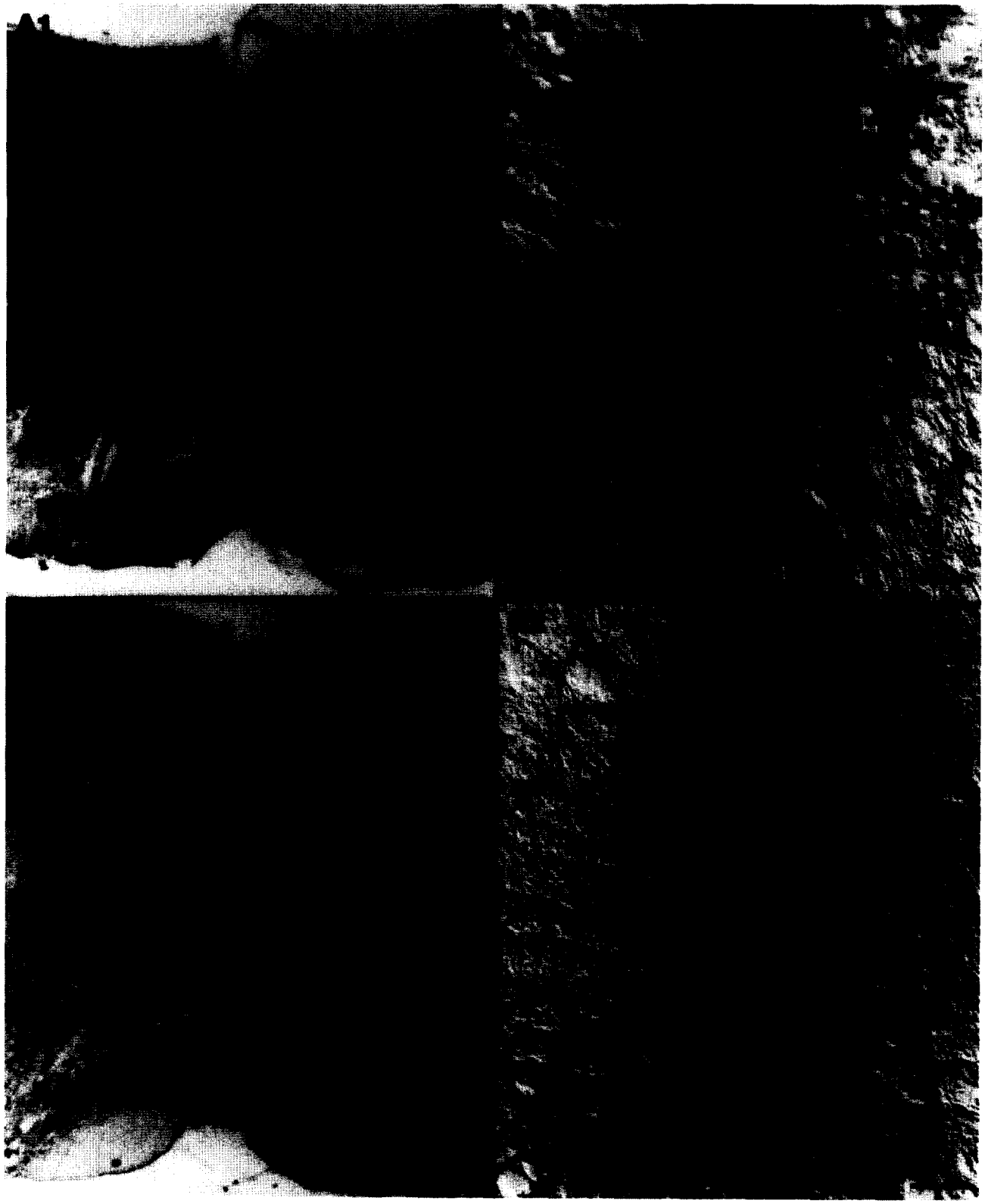

FIG. 3. Photomicrographs of representative sections showing TH-immunoreacted LC neurons at 8 weeks (A1 and A2) and 104 weeks of age (B1 and B2). A1 and B1 used bright-field optics (scale = 200 μm) and A2 and B2 used interference contrast optics (scale = 20 μm). Note the apparent maintenance in the numbers of 5HT+ neurons in the 104-week raphe relative to the 8-week raphe.

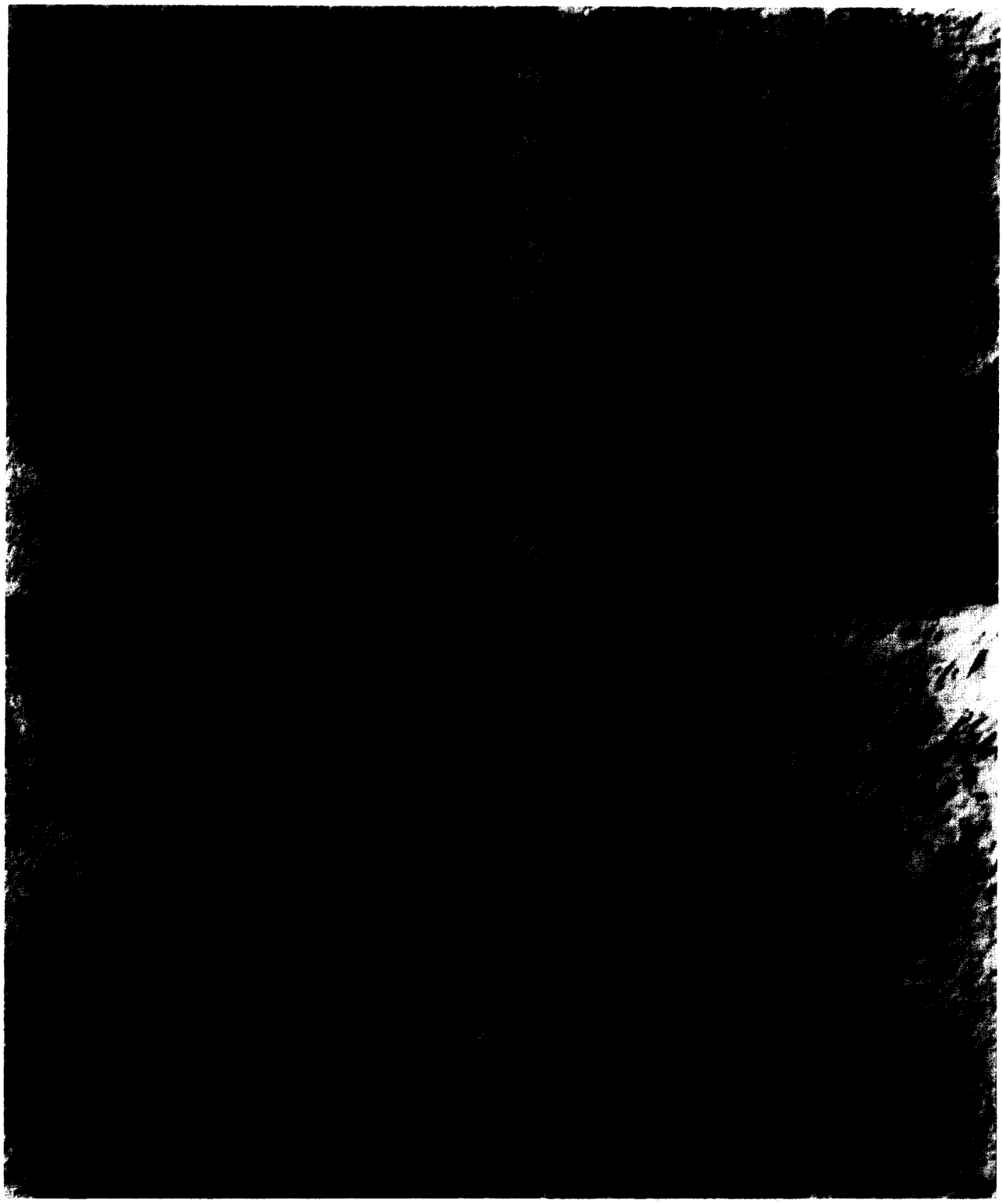

FIG. 4. Interference contrast photomicrographs of representative retinal whole mounts showing TH-immunoreacted retinal dopaminergic amacrine neurons at 8 weeks (A1 and A2) and 81 weeks of age (B1 and B2). A1 and B1 scale bar = 50 μm, A2 and B2 used scale bar = 10 μm. Note the relative maintenance in the numbers of TH+ neurons in the 81-week retina relative to the 8-week retina.

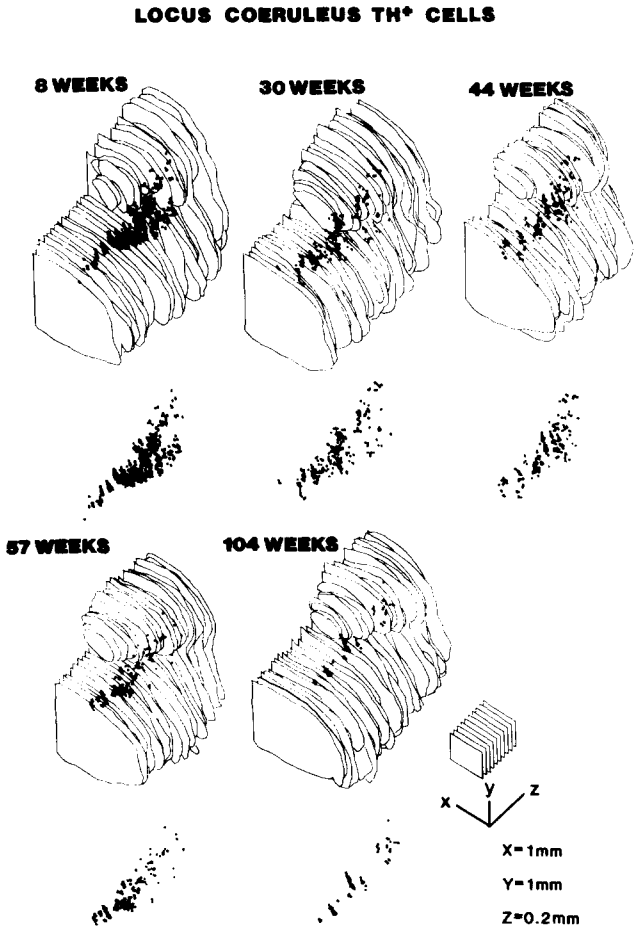

FIG. 5. Three-dimension distribution of TH+ somata in representative murine LC nuclei at five different ages. The somal locations are shown within the half brainstem outlines and are reproduced just below the outlines from the same perspective for clarity. A 10 times expanded scale was used in the Z dimension longitudinally along the brainstem relative to the dorsal-ventral Y dimension and medio-lateral X dimension. Note the apparent random and progressive deletion of TH+ somata with advancing age.

ysed according to a two stage procedure. Firstly, nonlinear estimation methods were used to determine the best coefficients for a number of different equation models that might fit the data (14) using programs developed by SYSTAT, Inc. (38). We used both Quasi-Newton and Simplex minimization methods to iteratively calculate the parameters and found that both methods gave almost identical results. Coefficients were computed for a number of models which might fit the data including linear [%Neurons = 100 (A(age in weeks) + B)], exponential [%Neurons = 100 ($e^{A(\text{age in weeks}) + B}$)], piecewise-linear [%Neurons = 100 r (A(age in weeks) + B + C(age in weeks − D) for age > D)] and piecewise-exponential models [%Neurons = %Neurons = 100 (($e^{A(\text{age in weeks}) + B}$) + ($e^{C(\text{age in weeks})}$ − D) for age > D)]. The coefficients for relationships with the minimal least squares values for the data points were taken for each of the models (15). The coefficients obtained from the nonlinear estimation procedures were then used to recompute Y axis values for the original data points in an attempt to linearize the plots for each of the estimated models. The linearized data was then fitted using linear regression analysis and the goodness of the linear fits was examined using linear regression coefficients as a second evaluation of the computed models. The counts were plotted together with 99% confidence limits for their mean values and slopes using the Statview SE programs developed by Brainpower, Inc.

RESULTS

Specific neuronal subtypes such as dopaminergic neurons in the substantia nigra compacta (SNc) or serotonergic raphe neurons in the brainstem midline are difficult to conclusively identify with nonspecific stains like Nissl or hematoxylin-eosin. For example, there are a number of different neuronal shapes and sizes in the SNc on Nissl staining, only two of which contain dopamine and project to the striatum (27). A particularly difficult problem for identification on Nissl stains is provided by the dopaminergic retinal amacrines. They make up a relatively small proportion of the neurons whose somata are located in the inner nuclear layer of the retina with an average density of 44.3 cells/mm^2 in the retina of 8-week-old C57 mice (33) and are indistinguishable on Nissl stains from the somata of other amacrine populations and bipolar cells. Locus coeruleus (LC) noradrenergic neurons are easier to identify on Nissl-stained sections since almost all of the neurons within the nuclear confines are projection neurons which contain both TH and dopamine beta hydroxylase (31).

In contrast, the above subtypes were easily identified using antibodies raised against TH or 5HT as is illustrated by the low and high power photomicrographs of immunoreacted sections for each of the four neuronal subtypes at 8 weeks and 81 or 104 weeks of age in Figs. 1–4. The monoaminergic neurons in the aged brains did not show a discernible decrease in immunoreaction density for either TH or 5HT compared to those from younger brains (compare the A2 and B2 panels of each of the Figs. 1–4). In fact, TH immunoreaction density of some LC and SNc somata in the aged animals often appeared to be increased relative to those in the younger animals [see (10)].

There was a decrease in the numbers LC TH+ and SNc TH+ somata and the numbers of TH+ processes within the two nuclei even when examining single sections like those illustrated in Figs. 1 and 2. In contrast, the average numbers of raphe 5HT+ neurons appeared unchanged over the range of ages we examined (Fig. 3). Examination of single sections or whole mounts alone was not sufficient to determine if there was a decrease in the numbers of dopaminergic retinal amacrines over the life span of the mice (Fig. 4).

Figure 5 presents representative examples of the three-dimensional localizations of LC TH+ somata on one side of the brainstem from computer reconstructions of alternate serial sections taken longitudinally along the brainstem. The reconstructions show a progressive, apparently spatially uniform loss of TH+ somata from the LC over the age range examined. We were able to rotate the reconstructions to any desired orientation and were unable to detect any preferential loci of TH+ somal loss within the LC. In contrast, some of the reconstructions suggested that relatively earlier loss might occur from the posterior portions of the SNc.

Figure 6 presents plots for the distributions of somata longitudinally along the long axis of the brainstem for the LC, SNc and raphe monoaminergic subtypes. Each point represents the number of somata for a single nucleus on a single transverse section. Each of the different symbols in A1–3, B1–3 and C1–3 represents the counts for a different animal so that graphs 1, 2 and 3 in each row of graphs present superimposed plots for four nuclei, each taken from a different animal at 8–20, 52–57 and 88–104 weeks of age, respectively. The sections were aligned for each animal against specific landmarks on the alternate Nissl

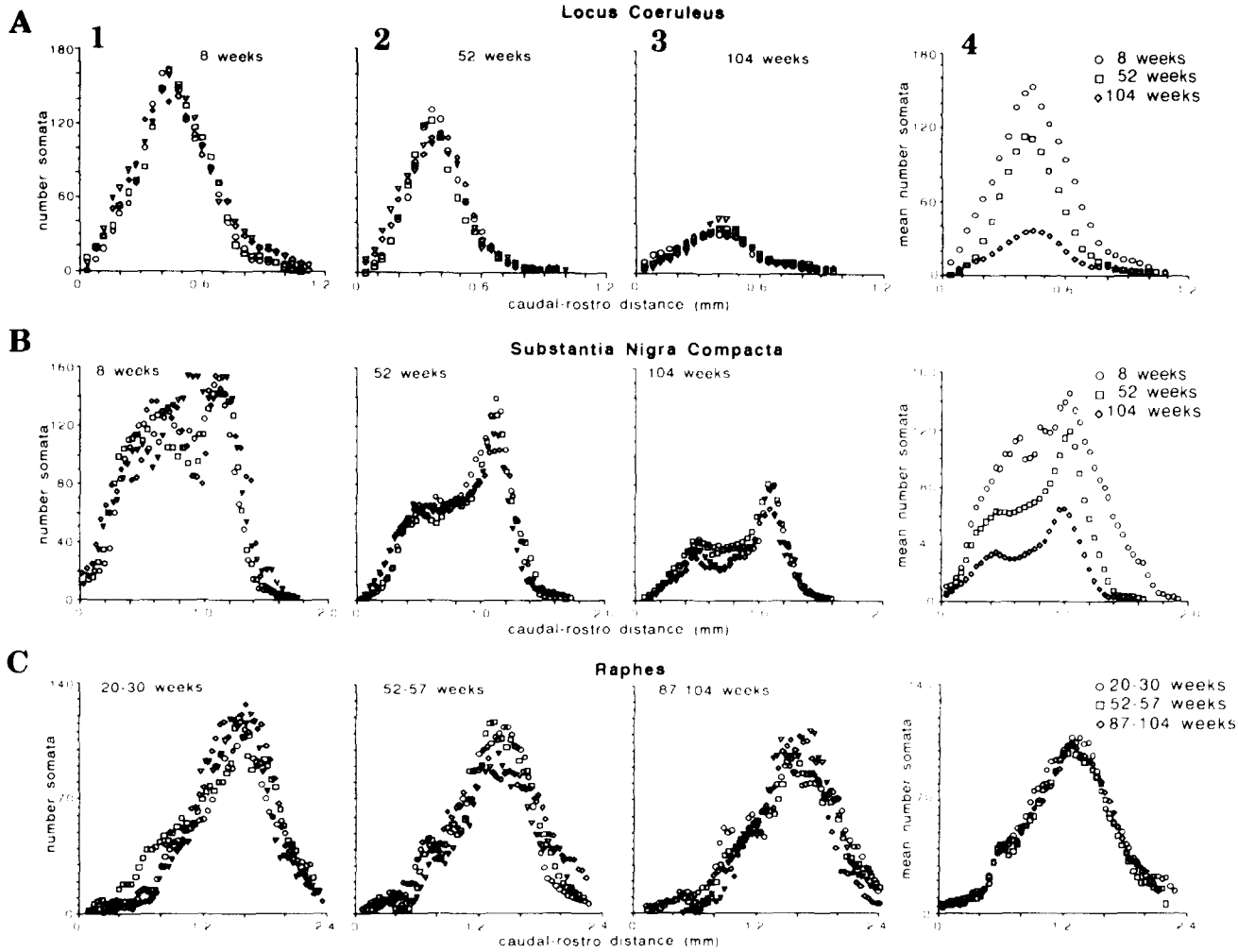

FIG. 6. Numbers of immunoreactive somata versus longitudinal position in the brainstem. The graphs in rows A, B and C are for LC, SNc and raphe nuclei respectively. Columns 1, 2 and 3 are labelled for progressively increasing ages. The abscissae are for length in mm along the brainstem aligned against specific reference structures. One nuclei in a different animal is represented by each symbol and four nuclei are overplotted in each graph. Column 4 presents graphs of average counts calculated for 10 nuclei with each of three ages represented by a different symbol.

sections so that the abscissa values are presented as longitudinal length along the brainstem. The fourth graph in each row presents average values for 8 different nuclei relative to brainstem length for the three ages of each neuronal subtype.

The plots reveal progressive loss of TH+ neurons in the LC (graphs 6A1–4) and SNc (graphs 6B1–4) with advancing age. In marked contrast, the plots for raphe 5HT+ neurons show minimal loss along the length of the nucleus which is only detectable on the average plots (graphs 6C1–4). The most striking result was the fact that the longitudinal distributions for different animals were similar for a given subtype at a given age. We therefore concluded that the probability of neuronal loss from different longitudinal portions of each nucleus was comparable for each isogenic animal. The TH+ neuronal loss from LC was similar from all longitudinal parts of the nuclei (graphs 6A1–4) as suggested by the three-dimensional reconstructions. In contrast, the distribution of loss in the SNC was more variable (graphs 6B1–4) and indicated that caudally located neurons might be relatively more vulnerable early in life (compare graphs 6B1 and 6B2).

Figure 7 presents representative nearest neighbor distributions for the retinal TH+ amacrine cells for three representative pairs of animals at different ages. The modes of the distributions shift to longer distances between nearest pairs as the animals age while maintaining a unimodal distribution with similar variance. The shifts can be interpreted to indicate loss of the TH+ amacrines according to a spatially uniform process similar to that found for the longitudinal distributions for the brainstem neurons. That is, the TH+ amacrines are deleted randomly from their matrix-like distribution in the retina without evidence of central or peripheral retinal predilection [see (33) for details on interpretation of nearest neighbor plots].

Table 1 presents means and standard deviations for the total counts in the three nuclei at 8 and 104 weeks of age and counts/mm^2 for the retinae at 8 and 88 weeks of age. These values are included to aid in the interpretation of Fig. 8 which presents our data for the four subtypes as a plot of the natural logarithm of the percentage of surviving neurons versus age in weeks. Each point represents the total counts taken from alternate sections through an entire nucleus or from an entire retinal whole mount

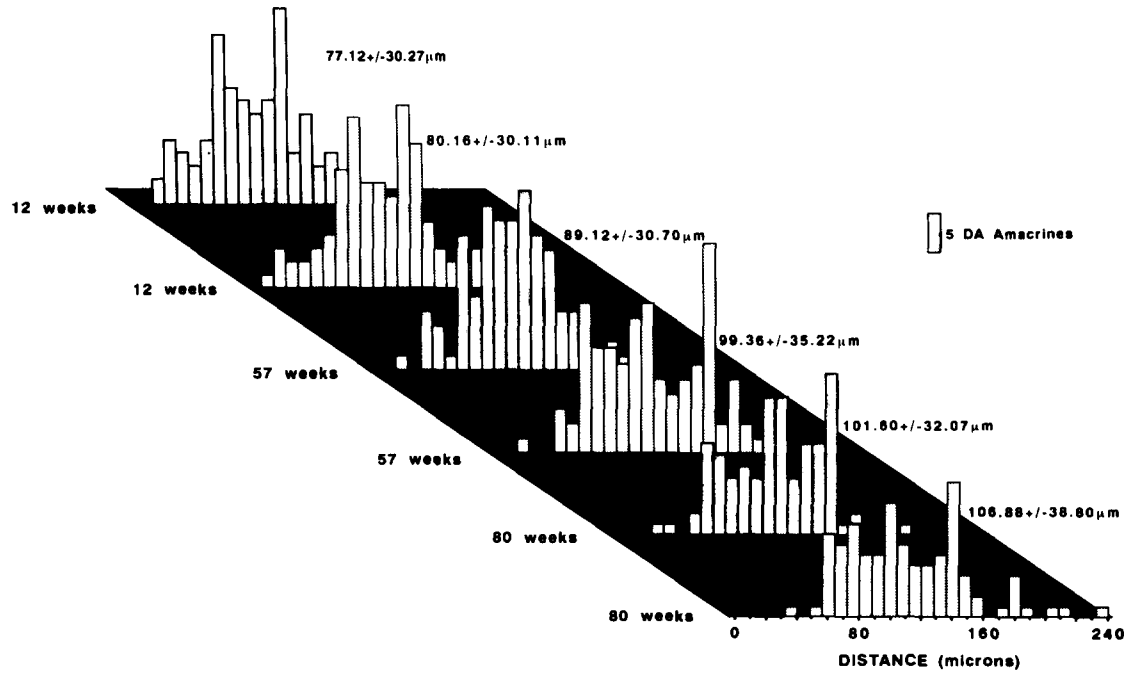

FIG. 7. Nearest neighbor analysis for TH+ retinal amacrines at three ages. The interval distributions present the distances between randomly chosen TH+ amacrine somata and their nearest TH+ amacrine soma. Two examples are presented at 12, 57 and 80 weeks. The values adjacent to the distributions present means ± standard deviations for each distributions. Note the progressive shift of the interval distribution means (and modes) to longer distances with advancing age while the standard deviations remain relatively unchanged.

in one animal and presents the values for each nucleus normalized to the mean values for the 8-week-old animals of the same subtype and expressed as percentages.

Table 2 presents the best coefficients and the least squares values for the nonlinear estimation fits and the linear correlation coefficients for the linear and log linear plots obtained for four of the different model equations we tested. For all four subtypes, the minimum least squares value was obtained for a simple exponential model. Piecewise equation models consistently gave higher loss function values than linear or exponential models. Similarly, maximum linear regression coefficient values were obtained for plots in which ordinate values were scaled to their natural logarithm as compared to linear, piecewise-linear models or piecewise-exponential models (two regression coefficients were calculated for the piecewise models, one for values less than the computed breakpoint value and second for values exceeding the computed breakpoint). Hence we concluded that the time course of the neuronal death could be best characterized by a single decaying exponential relationship and could be represented by semilogarithmic plots like Fig. 8. The exponential rate constants are shown on Fig. 8 and ranged from −0.001 for the raphe 5HT+ neurons to −0.15 for the LC TH+ neurons. DA retinal amacrines had an intermediate rate (−0.04) while SNc TH+ neurons had a similar rate (−0.013) to LC TH+ neurons.

Figure 9 presents the 99% confidence limits for the slopes (left-hand graph) and means (right-hand graph) of the semilogarithmic plots for each of the four neuronal subtypes. The decay parameters (parameter A in Table 1) as presented by the linear slopes for the four subtypes do not overlap at the level of the 99% confidence limits calculated for the slopes of the linear fits to the semilog plots (as shown by the inset values on the left-hand graph in Fig. 9). Similarly the 99% confidence limits for the means do not overlap. The slopes for the LC and the SNc TH+ counts were not significantly different ($p<0.05$) but the other slopes were all significantly different ($p<0.01$). The inset values on the the right-hand graph in Fig. 10 presents the + and − 99% intercepts for the 100 week of age lines and serve to illustrate that the mean percentage surviving neurons can be estimated to better than ±4% over the entire range of ages we examined for the four subtypes.

It is worthwhile to note that the mean values for the NIA mice that were sacrificed immediately on receipt from the supplier fell well within the 99% confidence limits determined for the genetically similar University of Calgary reared mice. This seems to indicate that rearing conditions peculiar to the University of Calgary facility are not responsible for the rates and time course of ARNL found in this study.

The decreases in numbers of TH+ and 5HT+ neurons with aging does not necessarily indicate neuronal death. For example, in studies directed toward understanding the action of the toxin MPTP on catecholaminergic neurons in C57 mice, we found that by 20 days a dose-dependent proportion of SNc and LC TH+ neurons were destroyed by the toxin (31). In contrast, a dose-dependent proportion of TH+ retinal amacrines underwent a complete loss of TH immunoreactivity and remained undetectable immunocytochemically for 6–9 months but then fully recovered their TH immunoreactivity. Similarly, the loss of the TH or 5HT immunoreactive subtypes with aging could result in part or all from a failure of the synthesis or modifications of the immune structure of the proteins or transmitters recognized by our antibodies.

We have previously utilized a method for comparing counts of TH+ somata and Nissl-stained somata in randomly chosen pairs of immediately adjacent sections to determine if a proportion of neurons in the LC are detectable with Nissl stain but no longer are synthesizing sufficient TH protein to be detectable

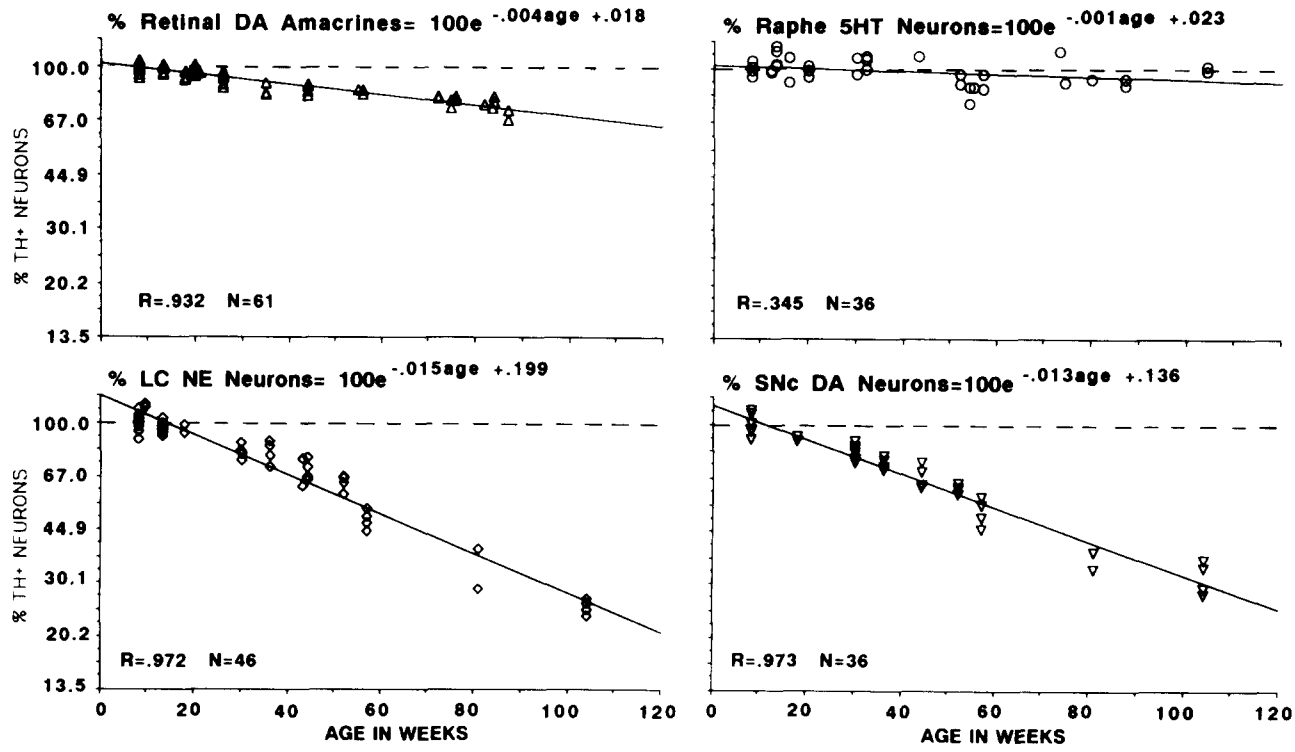

FIG. 8. Logarithm of percentage of remaining immunoreactive somata versus age in weeks. Each point is for the counts taken from alternate sections through a single nucleus or from an entire retinal whole mount and normalized as percentage from the mean value calculated for the eight-week-old animals. The ordinate scale is for the natural logarithm of the percentage counts. The best fit exponential equation is presented at the top of each graph. N = the number of nuclei and R = the linear regression coefficient.

immunocytochemically (31). Figure 10 presents plots for numbers TH+ somata (abscissa) and Nissl-stained neuronal somata on randomly chosen adjacent sections for LC neurons in 8-week-old and 57-week-old mice (four nuclei are pooled for each graph). The dashed line indicates the relationship for equal numbers of TH+ and Nissl-stained somata on adjacent sections while the solid line presents a linear regression fit to the data points. The plots are representative of those we have found for a variety of ages up to 104 weeks and show that the number of TH+ somata provide a good estimate of the number of Nissl-stainable LC neurons. The data can be criticized by the assertion that surviving LC neurons have both lost TH immunoreactivity and have atrophied to such an extent that they can no longer be distinguished from glia on somal size criteria.

Work in progress in our laboratory using the retrograde transport of fluorogold has not provided evidence for shrinkage of 104-week-old SNc neurons projecting to the striatum (P. Salo, personal communication) and in fact most of the TH+ somata hypertrophy by 10–30% in the aged animals (unpublished observations). If a similar maintenance or increase of somal size holds for the LC neurons with aging, then the relationships for LC TH+ neurons in Figs. 8 and 9 would provide a reliable estimate of neuronal death versus age. We have obtained similar results for TH+/Nissl plots of SNc somata (unpublished observations) but the wide dispersion and mixing of the retinal amacrine TH+ and the raphe 5HT+ neurons with other neuronal subtypes in the same structure made it difficult to apply the adjacent section comparison to those subtypes in order to conclusively demonstrate neuronal death [see Discussion section in (31)].

DISCUSSION

C57 black mice have been reported to have combined male-female mean survivals ranging from 78 to 127 weeks with most workers reporting 109 to 117 weeks (9,25). Hence we determined the neuronal numbers for the four subtypes over most of the average life span of the C57 strain. Some neuronal subtypes undergo so-called histogenetic death early in postnatal life which appears to be related to the neurons success in innervating target neurons [see (29)]. The neuronal subtypes in the youngest animals we studied (8 weeks of age) had completed their histogenetic death phases and it likely did not contribute to our findings.

We have shown that the rates of age-related neuronal loss for different immunocytochemically identified monoaminergic neuronal subtypes in the same animals can be fitted to a decaying

TABLE 1

COUNTS OF IMMUNOPOSITIVE SOMATA IN YOUNG ADULT AND AGED MICE

Neuronal Subtype Somata	Mean ± S.D Number or No./mm² Immunopositive 8 Weeks	84† or 104* Weeks
SNc TH+	3299 ± 261	1052 ± 132*
LC TH+	1592 ± 132	389 ± 20*
Raphe 5HT+	2332 ± 288	2237 ± 137*
Retinal Amacrine TH+	44.3 ± 1.7	33.7 ± 1.4†

TABLE 2

COEFFICIENTS AND LEAST SQUARES VALUES FOR NONLINEAR ESTIMATION

		Estimated Coefficients				Least Squares	Linear Regression
Model	Subtype	A	B	C	D	Value	Coef. (r)
Linear	LC TH+	−.009	1.081	none	none	0.242	.963
	SNc TH+	−.008	1.027	none	none	0.136	.960
	Ret. Am TH+	−.003	1.011	none	none	0.077	.926
	Raphe 5HT+	−.001	1.026	none	none	0.245	.117
Exponential	LC TH+	−.015	0.199	none	none	0.171	.972
	SNc TH+	−.013	0.136	none	none	0.098	.973
	Ret. Am TH+	−.004	0.018	none	none	0.067	.932
	Raphe 5HT+	−.001	0.023	none	none	0.238	.345
Piecewise linear	LC TH+	−.010	1.110	−.003	55.2	0.285	.871,.741
	SNc TH+	−.008	1.027	−.005	61.4	0.147	.851,.613
	Ret. Am. TH+	−.004	1.030	−.002	48.1	0.074	.901,.812
	Raphe 5HT+	−.002	1.020	−.001	45.2	0.248	.112,.115
Piecewise exponential	LC TH+	−.005	0.156	−.018	50.6	0.191	.813,.612
	SNc TH+	−.008	0.116	−.010	74.2	0.103	.722,.546
	Ret. Am. TH+	−.001	0.024	−.007	62.1	0.072	.812,.645
	Raphe 5HT+	−.001	0.016	−.002	39.2	0.244	.212,.183

exponential model. SNc dopaminergic and LC noradrenergic neurons showed similar exponential rate constants (−0.013 and −0.015 respectively) while the retinal DAg amacrines showed rates of loss (exponential rate constant of −0.004) that were about 30% of those for the SNc and LC neurons while the 5HT raphe neurons showed almost no loss over the period studied (exponential rate constant of −0.001). The fits were made to relatively large numbers of almost continuous data points so as not to be open to the criticisms that have been applied to fits of human data comprised of fewer points that were not continuous over the age range studied [see (19)]. Since the data did not fit to piecewise models as well as to linear or exponential models, it did not provide evidence for a lower rate of loss during early life and an accelerated rate late in life. In fact, our data revealed progressively smaller absolute losses of neurons as the animals aged and therefore differ from studies reporting increased rates of neuronal loss in the later stages of life. Some other workers (35) have assumed a piecewise linear model and fitted their data using linear regression methods according to an assumed breakpoint. The nonlinear estimation methods used in this study estimated both the best breakpoint and the coefficients for the piecewise models.

Numbers of LC neurons appear to decrease in humans in a similar manner to that in our C57BL mice (22,36). Yet the time

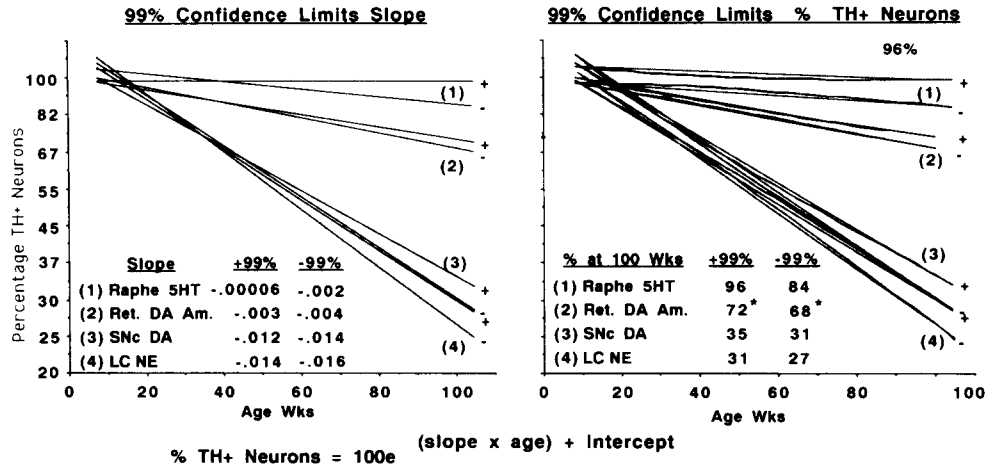

FIG. 9. Confidence limits for slopes and mean values of exponential rate of loss equations. The left-hand graph presents the 99% confidence limits for the slopes of the semilog plots for the four monoaminergic populations. The right-hand graph presents the 99% confidence limits for the mean values for the best fit linear regression equations for the semilog plots. Note there is no overlap in the 99% confidence limits for the slopes or the means for the four populations.

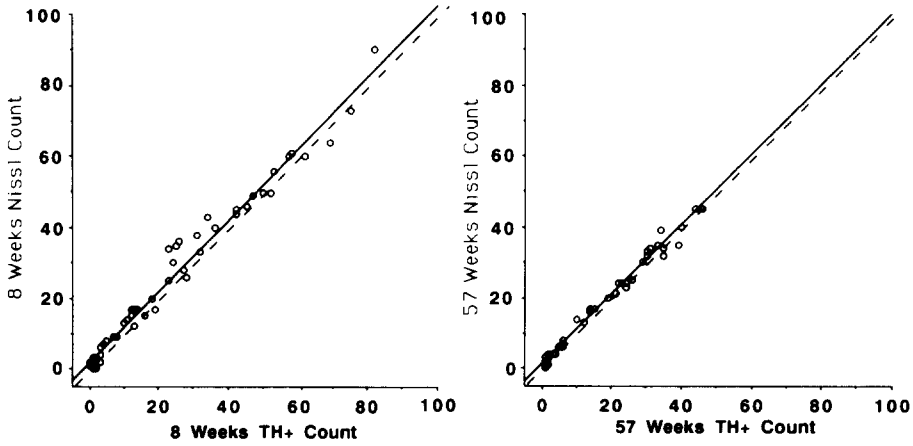

FIG. 10. Joint counts of LC neuronal somata in adjacent Nissl-stained and TH-immunoreacted somata. Each point represents the number or Nissl-stained neuronal somata (ordinates) and TH+ neuronal somata (abscissae) from immediately adjacent sections. Ten pairs of sections were chosen randomly for each nuclei and the data from four nuclei are pooled on each graph. The left-hand graph is for 8-week-old animals and the right-hand graph is for 57-week-old animals. The solid line presents a linear regression fit through the points while the dashed line demarcates the equal value diagonal.

course of loss differs from those reported for ASH/TO mice strain using hematoxylin-eosin staining (32) and in the Fischer 344 rat where LC neuronal numbers seem to remain constant to very late in life (8,28).

Substantia nigra neurons have been reported to decrease almost linearly during human life span (20) but C57 mice have been reported to show little or no loss by 24 months (21). Our values differ from theirs in terms of total counts as well. They used a random section selection method to estimate 8276 ± 367 TH+ somata per SNc nucleus at 3 months while we found 3299 ± 261 Th+ somata per nucleus at 8 weeks by counting from alternate sections through whole nuclei. Our counts are almost identical to those recently reported for TH+ SNc neurons in C57 mice at 2 months of age (12). To our knowledge there have been no previous examinations of the changes in the numbers of dopaminergic retinal amacrine neurons or serotonergic raphe neurons with aging.

Part of the reason for the relatively narrow 99% confidence levels for our data points may relate to the possibility that the immunocytochemical identification of the neurons allowed us to recognize neurons with similar genetic expression and possibly similar functional roles within the brain regions studied. The inbreeding of our mice and the relatively homogeneous rearing environments may also be relatively important factors in the small variances that we found.

Transmitter expression by itself does not seem to be a major determinant of the rates of neuronal loss since two dopaminergic subtypes, rAm and SNc neurons, showed markedly different exponential rates of ARNL. Similarly, axonal length does not seem to be a major determinant since the locally ramifying retinal amacrines had higher rates than the raphe neurons and lower rates than LC neurons, both of which have long and extensively projecting axons. The present study does not provide any insights into the molecular or cellular processes that might determine the different rates of loss of the four subtypes other than to indicate that one or more processes causing loss of transmitter-identified neuronal subtypes are operative throughout most of the life span of the animals. One could consider a variety of trophic and toxic mechanisms that might operate over the entire life span and influence the neuronal subtypes differentially [see (2) for a review]. According to the exponential fits, each subtype loses a constant proportion of the remaining neurons at all ages and the subtypes differ according to the proportion lost per unit time period. Furthermore, our data shows that LC neurons are lost uniformly from all portions of the nuclei and that dopaminergic retinal amacrines are lost randomly from the retina. This is particularly interesting for the LC since different cephalo-caudal portions of the nucleus project to different spinal, cerebellar and forebrain target tissues (11). Hence LC neurons projecting to one target tissue did not appear to have higher rates of ARNL than those projecting to others. In contrast, SNc dopaminergic neurons in the caudal part of the nucleus seems of have a higher probability of loss early in life.

Our data indicates that the loss of LC TH+ neurons likely represents death of those neurons. Yet the loss of the TH+ SNc or rAm neurons could in part reflect a marked reduction in TH protein synthesis, an increase in the rate of TH degradation or a change in the configuration of the TH molecule so that it no longer is recognizable by our antibodies. Similar changes could be postulated for key molecules for 5HT synthesis relative to the loss of the raphe 5HT+ neurons. Marked reductions in neuronal TH concentrations would likely render the neurons incapable of dopaminergic transmission to their postsynaptic neurons and would therefore have similar functional consequences to neuronal death in terms of transmission to their postsynaptic target neurons [see (33)]. That is, the neurons would remain within the tissues but would not participate in neuronal circuit operation. Abnormalities in transcription and overall decreases in mRNA expression have been hypothesized to contribute to neuronal aging, although to date there have been few studies of the transcriptional, translational or posttranslational processes as they apply to specific proteins in aging neurons [see (5) for a review]. Data included in a companion manuscript (10) indicates that aging SNc neurons increase their TH immunodensity per unit somal volume and per average somata which may offer a preliminary indication that TH protein synthesis is increased rather than decreased in aging neurons and that the synthesis of different proteins may be affected differently with aging.

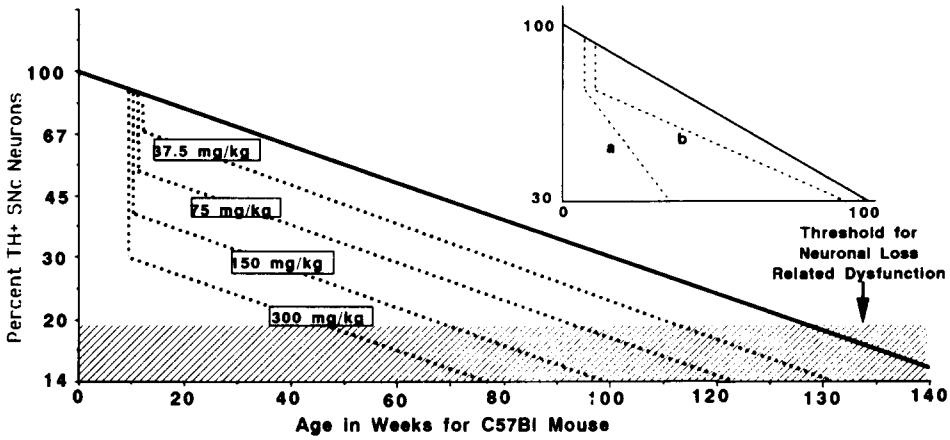

FIG. 11. Schematic representation of interaction among toxic neuronal loss, age-related neuronal loss and threshold concept for behavioral deficits in aging. The solid line in the main graph presents the ARNL relationship determined for SNc TH+ neurons in the present study. The vertically oriented dotted lines at 8 weeks of age present the mean loss of SNc TH+ neurons caused by the doses of MPTP shown [taken from (31)]. The continuations of the the dotted lines are meant to represent the joint age-related and toxically induced neuronal loss that would occur if the rate of ARNL was not altered by the toxic exposure in early life. The shaded area represents the hypothetical 20% threshold for behavioral deficits with neuronal loss. The inset diagram is included to note our recognition that early toxic exposure could also accelerate (dotted line a) or slow (dotted line b) the rate of ARNL.

The different rates of age-related loss of the four monoaminergic neuronal subtypes in these isogenic mice will offer multiple models in the same animal to uncover subcellular and molecular mechanisms that contribute to those rates. It will be particularly interesting to compare the time courses and rates of ARNL for the four subtypes in the C57BL mouse to other murine strains and to discover the relationship, if any, between longevity and rates of ARNL (39). At present, we do not know whether longevity and rates of ARNL are influenced by common chromosomal regions (7).

A number of workers have proposed that behavioral deficits relating to the loss of SNc neurons do not become evident until a threshold loss of approximately 80% of the neurons has been exceeded [see (1) for an example]. Accepting the concept of the 80% loss threshold and applying it to other neuronal subtypes, behavioral deficits would not become apparent for behaviors that are dependent on the SNc dopaminergic, raphe 5HT neurons, dopaminergic retinal amacrines and the LC noradrenergic neurons until 133, 1612, 407 and 116 weeks of age respectively. Hence the only ARNL-related deficits that could occur within the probable life span of the C57BL/6 mice would result from the loss of SNc dopaminergic or LC noradrenergic neurons.

Most neurodegenerative diseases first become clinically evident in late life. Calne and Langston (3) have proposed that the late onset of Parkinson's disease results from toxic exposure early in life which destroys a proportion of the SNc dopaminergic neurons but that clinical deficits do not become evident until ARNL causes a further loss of neurons sufficient to exceed an 80% threshold. We recently have shown that the Parkinson's-like toxin, MPTP, produces a dose-dependent destruction of SNc and other catecholaminergic neurons in the C57BL mouse (31). Losses of up to 70–80% of SNc neurons in the C57BL mice due to MPTP exposure do not result in immediate Parkinsonian motor deficits in keeping with the threshold concept (30). Figure 11 schematizes the ARNL relationship we have found for SNc dopaminergic neurons together with the average dose-dependent losses we found for SNc when the animals were exposed to various doses of MPTP at 8 weeks of age. The figure illustrates the Calne-Langston hypothesis and predicts the ages at which the animals would be expected to evidence Parkinson's-like movement deficits depending on the dose of toxin they received at 8 weeks of age. The hypothesis assumes that the rate of age-related loss would remain the same in animals exposed to the toxin as that in unexposed animals. That is, the toxic and age-related causes of neuronal loss would simply be additive. The inset graph in Fig. 11 is included to show how early toxic exposure might accelerate (dotted line a) or slow (dotted line b) the rates of ARNL we have found for the SNc DAg neurons and thereby advance or delay the ages at which Parkinsonian deficits appeared in the MPTP treated mice so that the toxic and age-related losses would be interactive rather than just additive.

A number of studies have reported only small or minimal changes in murine striatal dopamine concentrations [see (24) for a review] or D2 receptor densities [see (18) for a review] with aging. In general, those studies have not taken the possible loss of either the presynaptic SNc neurons or the postsynaptic striatal neurons into account. If dopamine synthesis and release or D2 receptor density remained constant for each remaining neuron with aging, then target tissue transmitter concentrations should reflect the rates of ARNL for the SNc neurons and D2 receptor density should relate to the overall loss of both SNc neurons and their postsynaptic striatal partners. A companion paper (10) reports that aging SNc TH+ neurons in the C57BL/6 mice increase their dopamine content on average compared to younger animals and that dopamine synthesis may be increased in proportion to the age-related loss of their fellows. Increased dopamine synthesis by the aging SNc neurons appears to explain the finding that striatal dopamine concentrations remain unchanged or decrease only slightly across the life span of mice despite marked age-related loss of TH+ SNc neurons and illustrates the need to take age-related neuronal loss into account in interpreting specific subcellular or molecular changes that accompany brain aging.

ACKNOWLEDGEMENTS

The research was supported by Medical Research Council of Canada grant MA-5218 and a Parkinson Foundation of Canada grant. We are grateful to Nadine Seniuk, Montgomery Martin and Sandra Richardson for helpful suggestions.

REFERENCES

1. Agid, Y.; Blin, J. Nerve cell death in degenerative diseases of the central nervous system:clinical aspects. In: Bock, M., ed. Selective neuronal death. Chichester: John Wiley and Sons; 1987:3–18.
2. Azmitia, E. C.; Whitaker-Azmitia, P. M.; Bartus, R. Use of tissue culture models to study neuronal regulatory trophic and toxic factors in the aged brain. Neurobiol. Aging 9:743–758; 1988.
3. Calne, D. B.; Langston, J. M. Etiology of Parkinson's disease. Lancet 2(8365–8366):1457–1459; 1983.
4. Coleman, P. D.; Flood, D. G. Neuron numbers and dendritic extent in normal aging and Alzheimer's disease. Neurobiol. Aging 8:521–545; 1987.
5. Finch, C. E.; Morgan, D. G. RNA and protein metabolism in the aging brain. Annu. Rev. Neurosci. 13(75):75–87; 1990.
6. Flood, D. G.; Coleman, P. D. Neuron numbers and sizes in aging brain: Comparisons of human, monkey, and human data. Neurobiol. Aging 9:453–463; 1988.
7. Gelmon, R.; Watson, A.; Bronson, R.; Yunis, E. Murine chromosomal regions correlated with longevity. Genetics 118:693–704; 1988.
8. Goldman, G.; Coleman, P. D. Neuron mumbers on locus coeruleus do not change with age in Fisher 344 rat. Neurobiol. Aging 2:33–36; 1981.
9. Goodrick, C. L. Life-span and the inheritance of longevity of inbred mice. J. Gerontol. 30(3):257–263; 1975.
10. Greenwood, C. E.; Tatton, W. G.; Seniuk, N. A.; Biddle, F. E. Increased dopamine synthesis in aging substantia nigra neurons. Neurobiol. Aging 12:557–565; 1991.
11. Grzanna, R.; Molliver, M. E. The locus coeruleus in the rat: an immunohistochemical delineation. Neuroscience 5:21–40; 1980.
12. Gupta, M.; Schwarz, J.; Chen, X. L.; Roisen, F. J. Gangliosides prevent MPTP toxicity in mice—an immunocytochemical study. Brain Res. 527:330–334; 1990.
13. Heumann, D.; Leuba, G. Neuronal death in the development and aging of the cerebral cortex of the mouse. Neuropathol. Appl. Neurobiol. 9:297–311; 1983.
14. Hoaglin, D. C.; Mosteller, F.; Tukey, J. W. Understanding robust and exploratory data analysis. New York: John Wiley and Sons, Inc.; 1983.
15. Jennrich, R. I.; Moore, R. H. Maximum likelihood estimation by means of nonlinear least squares. In: Proceedings of the statistical computing section, American Statistical Association. 1975:57–65.
16. Kawamura, Y.; Okazaki, H.; O'Brien, H.; Dyck, P. J. Lumbar motoneurons of man. 1. Number and diameter histogram of alpha and gamma axons of ventral root. J. Neuropathol. Exp. Neurol. 36: 853–860; 1977.
17. Konigsmark, B. W. Methods for the counting of neurons. In: Nauta, W. H.; Ebesson, S. O. E., eds. Contemporary research methods in neuroanatomy. New York: Springer-Verlag; 1970:315–380.
18. Leprohon-Greenwood, C. E.; Cinader, B. Variations in age-related decline in striatal D2 dopamine receptors in a variety of mouse strains. Mech. Ageing Dev. 38:199–206; 1987.
19. McGeer, P. L.; Itagaki, S.; Akiyama, H.; McGeer, E. G. Comparison of neuronal loss in Parkinson's disease and aging. In: Calne, D. C. D. B.; Comi, G.; Horowski, R., eds. Parkisonism and aging. New York: Plenum; 1989:25–34.
20. McGeer, P. L.; McGeer, E. G.; Suzuki, J. S. Aging and extrapyramidal function. Arch. Neurol. 34:33–35; 1977
21. McNeill, T. H.; Koek, L. Differential effects of advancing age on neurotransmitter cell loss of the substantia nigra and striatum of C57BL/6N mice. Brain Res. 521:107–117; 1990.
22. Mann, D. M. A. The locus coeruleus and its possible role in ageing and degenerative disease. Mech. Ageing Dev. 23:73–94; 1983.
23. Mesulam, M. M.; Mufson, E. J.; Rogers, J. Age-related shrinkage of cortically projecting cholinergic neurons: A selective effect. Ann. Neurol. 22:31–36; 1987.
24. Morgan, D. G.; Finch, C. E. Dopaminergic changes in the basal ganglia: A generalized phenomenon of aging mammals. Ann. NY Acad. Sci. 515:145–160; 1988..
25. Myers, D. D. Review of disease patterns and lifespan in ageing mice: genetic and environmental interactions. In: Bergsma, D.; Harrison, D., eds. Birth defects. New York: Alan Liss; 1978:41–53.
26. Nieuwenhuys, R. Chemoarchitecture of the brain. Berlin: Springer-Verlag. 1985.
27. Poirier, L. J.; Giguere, M.; Marchand, R. Comparative morphology of the substantia nigra and the ventral tegmental area in the monkey, cat and rat. Brain Res. Bull. 11:371–397; 1983.
28. Reis, D. J.; Ross, R.; Joh, T. H. Changes in the activity and amounts of enzymes synthesizing catecholamines and acetylcholine in brain, adrenal medulla and sympathetic ganglia of aged rat and mouse. Brain Res. 136:465–474; 1977.
29. Rootman, D. S.; Tatton, W. G.; Hay, M. Postnatal histogenetic death of rat forelimb motoneurons. J. Comp. Neurol. 199:17–27; 1981.
30. Seniuk, N. A. Neuronal destruction by MPTP: Neurochemical and behavioral compensation by surviving neurons. Ph.D. Thesis, University of Toronto, 1989.
31. Seniuk, N. A.; Tatton, W. G.; Greenwood, C. E. Dose-dependent destruction of the coeruleus-cortical and nigral-striatal projections by MPTP. Brain Res. 527:7–20; 1990.
32. Sturrock, R. R.; Rao, K. A. A quantitative histological study of neuronal loss from the locus coeruleus of aging mice. Neuropathol. Appl. Neurobiol. 11:55–60; 1985.
33. Tatton, W. G.; Kwan, M. M.; Verrier, M. C.; Seniuk, N. A.; Theriault, E. MPTP produces reversible disappearance of tyrosine hydroxylase containing retinal amacrine cells. Brain Res. 527:21–32; 1990.
34. Terry, R. D.; DeTeresa, R.; Hansen, L. A. Neocortical cell counts in normal human adult aging. J. Neurol. Sci. 34:213–219; 1987.
35. Tomlinson, B. E. The numbers of limb motor neurons in the human lumbosacral cord throughout life. J. Neurol. Sci. 34:213–219; 1977.
36. Vijayashankar, N.; Brody, H. A quantitative study of the pigmented neurons in the nuclei locus coeruleus and subcoeruleus in man as related to aging. J. Neuropathol. Exp. Neurol. 38(5):490–497; 1979.
37. Walker, L. C.; Kitt, C. A.; Struble, R. G.; Wagster, V. M.; Price, D. L.; Cork, L. C. The neural basis of memory decline in aged monkeys. Neurobiol. Aging 9:657–666; 1988.
38. Wilkinson, L., SYSTAT: The system for statistics. Evanston, IL: Systat, Inc.; 1987.
39. Yunis, E. J.; Watson, A. L. M.; Gelmon, R. S.; Sylvia, S. J.; Bronson, R.; Dorf, M. E. Traits that influence longevity in mice. Genetics 108:999–1011; 1984.